Journal of The Electrochemical Society, 2022 **169** 060524

Electrochemical Stability and Reversibility of Aqueous Polysulfide Electrodes Cycled Beyond the Solubility Limit

Menghsuan Sam Pan,[1] Liang Su,[1] Stephanie L. Eiler,[1] Linda W. Jing,[1] Andres F. Badel,[1,2] Zheng Li,[3,*] Fikile R. Brushett,[2,*] and Yet-Ming Chiang[1,z]

[1]*Department of Materials Science and Engineering, Massachusetts Institute of Technology, Cambridge, Massachusetts 02139, United States of America*
[2]*Department of Chemical Engineering, Massachusetts Institute of Technology, Cambridge, Massachusetts 02139, United States of America*
[3]*Department of Mechanical Engineering, Virginia Tech, Blacksburg, Virginia 24061, United States of America*

Batteries which use dissolved redox-active species, such as redox flow batteries (RFBs), are often considered to be constrained in their operation and energy density by the solubility limit of the redox species. Here, we show that soluble redox active electrolytes can be reversibly cycled deeply into the precipitation regime, permitting higher effective concentrations, energy densities, and lower costs. Using aqueous sodium polysulfide negative electrolytes cycled in the nominal Na_2S_2 to Na_2S_4 capacity range as an example, we show that the effective solubility can be increased from 5 M in the fully-dissolved state to as much as 10 M using the precipitation strategy. Stable cycling was observed at 8 M concentration over more than 1600h at room temperature. We also analyze the range of polysulfide electrochemical stability, and characterize the precipitate composition. This enhanced effective concentration approach may be generalized to other redox chemistries that utilize solubilized reactants, and may be especially useful for long-duration storage applications where slow charge-discharge rates allow equilibration of precipitated species with the redox-active solution.

 [DOI: 10.1149/1945-7111/ac7669]

Manuscript submitted January 3, 2022; revised manuscript received April 28, 2022. Published June 17, 2022.

Supplementary material for this article is available online

The levelized costs of electricity (LCOE) for wind and solar electricity generation have dropped to a levels nearly competitive with that of fossil fuels, increasing the urgency for energy storage that can make intermittent generation dispatchable.[1,2] Accordingly, low-cost energy storage systems may enable greater adoption of renewable energy sources.[3–5] Recent use-case studies show that installed storage system costs of <$50/kWh are needed to span historical troughs in wind and solar generation, which typically reach durations of several days, and to provide reliable electricity at LCOE competitive with natural gas.[6] To reach such costs, it is critical to leverage energy storage compounds that are not reliant on resource-constrained elements such as cobalt and nickel. To this end, aqueous polysulfide electrolytes are an attractive option, due to the abundance and ultra-low cost of elemental sulfur ($\sim\$0.25\ kg)^{-1}$.[7] (In this paper we refer to the redox-active solutions as "electrolytes" in keeping with terminology for flow batteries.) Several aqueous sulfur based chemistries such as polysulfide/bromine,[8,9] polysulfide/polyiodide,[10,11] polysulfide/ferrocyanide,[12] lithium metal/polysulfide,[13] and polysulfide/lithium intercalation compounds[14,15] have been proposed and demonstrated in static or redox flow battery (RFB) configurations. The lowest-cost sulfur alternative to date, from the viewpoint of the chemical cost of stored energy, is the air-breathing aqueous sulfur RFB, recently demonstrated by our group using both lithium and sodium as the working ion.[16] Upon applying a techno-economic model, it is observed that the costs of the auxiliary components required to store the aqueous polysulfide electrolyte (e.g., tanks, supporting electrolyte salts) can easily exceed the cost of the redox-active materials, as shown in Fig. 1a. Therefore, increasing the capacity density (Ah/L) of the polysulfide electrode directly reduces the cost of storage, in addition to increasing energy density. Several previous attempts to increase capacity density have been made. Licht and Permunage utilized a reservoir of extra solid elemental sulfur or potassium sulfide, which dissolves into the aqueous polysulfide solution as the cell discharged; however, only discharging of the batteries were demonstrated in both cases.[17,18] Visco et al. enhanced the solubility of polysulfide species by introducing nonaqueous solvents into aqueous polysulfide electrolytes; the impact of the nonaqueous solvents on the energy storage cost, however, was not closely examined.[19]

As shown in Fig. 1a, an aqueous polysulfide electrolyte exhibits a low cost per stored capacity of <$5/kAh, and approaching $3/kAh for high sulfur concentrations. Assuming a 1 V operating voltage, this corresponds to an energy cost <$5/kWh for the aqueous polysulfide half-cell. While full system costs have not been modeled in the present work, a half-cell cost of this magnitude is promising for achieving a system cost of <$20/kWh as targeted in the U.S. Department of Energy's Energy Earthshot Initiative.[20]

In principle, increasing the capacity density of aqueous polysulfide electrodes can be accomplished by (1) increasing sulfur utilization by widening the polysulfide speciation range; and/or (2) increasing the solubility or effective solubility. Figure 1b illustrates these two effects on the capacity density of the polysulfide electrode. In this work, we first examine the stability of polysulfide solutions as a function of speciation, seeking the widest speciation range that is still stable enough for extended cycling. Then, the feasibility of cycling the polysulfide electrode deeply into the precipitation regime is examined. Finally, the chemical speciation of the precipitated sodium polysulfide co-existing with the redox-active solution is characterized.

Experimental

Preparation of aqueous sodium polysulfide solutions.—To preserve the integrity of air sensitive chemicals, sodium sulfide anhydrous (Na_2S, ⩾ 95%, Alfa Aesar) and sulfur (S, ⩾ 99.5%, Alfa Aesar) were dried under vacuum overnight and stored in an Ar-filled dry glovebox with O_2 and H_2O levels below 0.1ppm. Sodium hydroxide pellets (NaOH, ⩾ 98%, Alfa Aesar) were placed under vacuum overnight and stored in an Ar-filled wet glovebox. Aqueous Na_2S_4 solutions of various concentrations were prepared with the following steps. First, 3 M NaOH was dissolved into deionized water in the wet glovebox. (All aqueous polysulfide solutions in this work used 3 M NaOH as the supporting electrolyte.) Second, stoichiometric amounts of Na_2S and S in a 1:3 molar ratio were transferred within a sealed bottle from the dry glovebox into the wet glovebox. Third, the Na_2S and S powders were dissolved into the prepared 3 M NaOH solutions, using magnetic stirrers. Aqueous

*Electrochemical Society Member.
[z]E-mail: ychiang@mit.edu

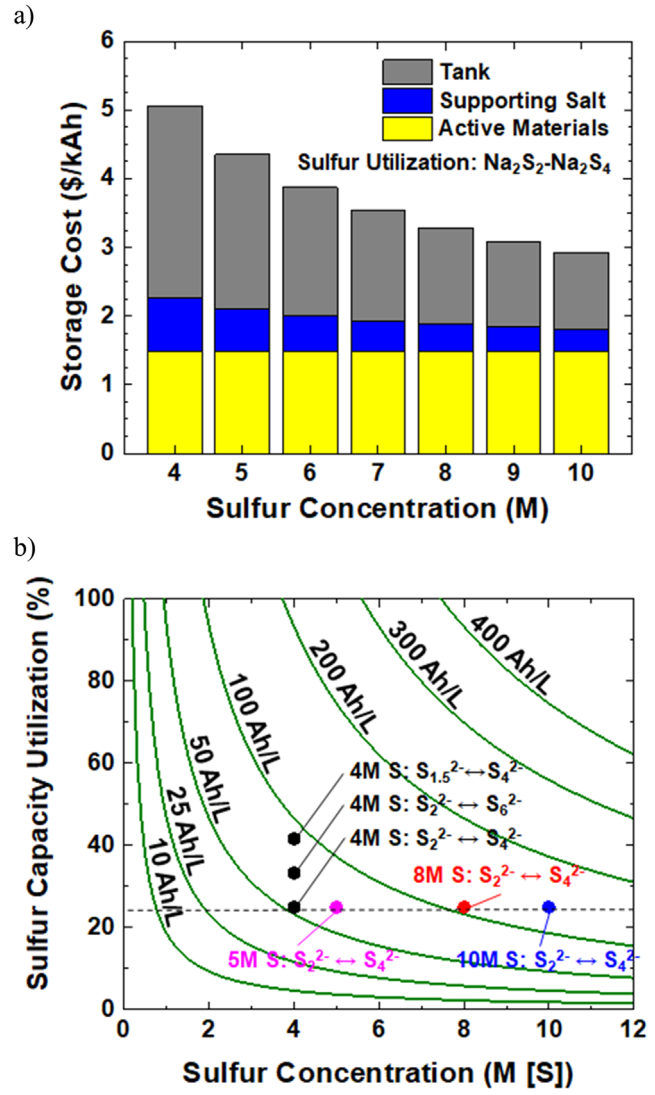

Figure 1. (a) Costs per stored capacity ($/kAh) for aqueous sodium polysulfide electrolytes of various concentrations assuming capacity utilization of Na_2S_2 to Na_2S_4, or 25% of theoretical sulfur capacity. Results are computed using the model in Ref. 16. The tank and supporting electrolyte components represent a large fraction of the cost, but their contribution diminishes as the sulfur concentration increases. (b) Sulfur capacity utilization, i.e., the redox speciation range, and the absolute sulfur concentration both affect the capacity density. Contours of constant capacity density are shown. The dashed horizontal line corresponds to the speciation range Na_2S_2 to Na_2S_4. The labeled points represent experiments conducted in this work, using Na^+ as the cation, except for the 5 M data point, which is from Ref. 16 and uses Li^+ as the cation.

sodium polysulfide solutions were stored and used in the wet glovebox to prevent polysulfide oxidation by O_2.[21] All cell assembly operations described below were performed in the wet glovebox.

Galvanostatic cycling of aqueous polysulfide electrodes.—The sulfur electrochemical reactions corresponding to full utilization of the sulfur theoretical capacity and cycling over a reduced capacity range (25%) are shown in Eqs. 1 and 2, respectively:

$$\text{Full Capacity: } S(s) + 2e^- \rightarrow S^{(2-)}(aq) \quad [1]$$

$$\text{Partial Capacity: } S_4^{(2-)}(s) + 2e^- \rightarrow 2S_2^{(2-)}(aq) \quad [2]$$

Modified H-cells, Fig. S1a (available online at stacks.iop.org/JES/169/060524/mmedia), were used for cycling experiments. The working chamber is modified to have a reduced volume to enable deep cycling of the electrolyte within. To eliminate crossover of species other than the sodium working ion, discs of a sodium superionic conductor (NaSICON, Ceramatec, Salt Lake City, Utah, USA), were used to separate the working and counter electrolytes. For some fully-soluble electrolyte cycling experiments, Nafion® perfluorinated membranes (Nafion® 117, 0.007' thickness, Sigma Aldrich) were used in place of the NaSICON. In all experiments, 200 μl of a desired concentration of Na_2S_4 solution was loaded into the low-volume side of the cells as the working electrolyte, while 5 ml of 2 M Na_2S_4 solutions was used as the counter electrolyte. Stainless steel mesh (316, Alfa Aesar) was used as the current collector on both sides of the cell. For all long-duration cycling experiments, a current of 1 mA, or 0.79 mA $cm^{-2}_{membrane}$, was used during charging and discharging with capacity cutoffs corresponding to sulfur state of charge (SOC) swings between the desired ranges. These capacity cutoffs are calculated from the sulfur concentration of the polysulfide solution and the volume of the working electrolyte (200 μl). Voltage was measured between the working electrolyte current collector and a Pt wire (≥ 99%, Alfa Aesar) immersed in the counter electrolyte as a pseudo-reference electrode. All cycling tests were performed using a VMP3 potentiostat (Bio-Logic).

Measurement of sodium polysulfide solubility in alkaline solution as a function of stoichiometry.—The solubility of Na_2S_x in alkaline solution varies with x, corresponding to the sulfur oxidation state and the state-of-charge (SOC) of the batteries discussed. The room-temperature solubility of Na_2S, Na_2S_2, Na_2S_3, Na_2S_4, and Na_2S_5 was measured by mixing Na_2S and S in the desired stoichiometric ratios, along with sodium hydroxide powder (NaOH, ≥ 98%, Alfa Aesar) and deionized water, to produce samples (10 ml volume) of 3 M NaOH concentration oversaturated with the sodium polysulfide. A wet glovebox held at temperature of 22.5 °C was used. The calculated oxidation state of sulfur in such solutions represents an average value, since aqueous sodium polysulfide solutions comprise a complex chemical equilibrium amongst Na^+, OH^-, HS^-, S^{2-}, S_x^{2-}, and other species.[22,23] The initially oversaturated solutions were stirred with magnetic stirrers for 24 h before adding 0.1 ml of 3 M NaOH solution every 24 h while stirring, until all solids were fully dissolved. The concentrations at which the solids were observed to be fully dissolved correspond to the solubility limits. Each solubility measurement was performed three times, and the mean values are reported along with the maximum deviation from the mean as the error limits.

Polysulfide precipitate characterization.—A modified H-cell with large enough electrolyte volume for direct observation of precipitation and extraction of precipitates for XPS analysis was used, Fig. S1b. 2.5 ml of 2 M Na_2S_4 solution was loaded into the modified side of the cells as the working electrolyte, while the counter electrolytes and reference electrodes were the same as described above. Precipitation was induced upon reduction of the solution from Na_2S_4 to Na_2S_2 under galvanostatic current of 1.97 mA $cm^{-2}_{membrane}$ (C/106 rate), while monitoring voltage between the working electrode and the Pt pseudo-reference electrode using a Solartron 1470E Potentiostat (Ametek Scientific Instruments, Berwyn, Pennsylvania, USA). After the reduction step, the cells were disassembled in the wet glovebox and the polysulfide precipitates were extracted. Excess solution was drained using filter paper and the precipitates were then dried under vacuum at room temperature for 5 h. The dried precipitates were ground into powder using an agate pestle and mortar in a dry glovebox, and then further dried under vacuum overnight. Grinding the precipitate allows XPS, a surface sensitive technique, to obtain information regarding the bulk of the precipitates. The powders were then transferred into a

Versaprobe II X-ray Photoelectron Spectrometer (Physical Electronics, Chanhassen, Minnesota, USA) using an Ar-filled transfer vessel. The XPS spectrometer used a monochromatic Al Kα X-ray source with 200 μm beam diameter and 49.3 W of X-ray power, and a dual-beam neutralizer to prevent charging. The XPS spectra obtained were calibrated, fitted, and quantified using CasaXPS (Casa Software Ltd, Wilmslow, Cheshire, UK) software. The spectra were charge-corrected by shifting the adventitious C 1 s peak to 284.0 eV and background-subtracted using a Shirley background.[24]

Results and Discussion

Assessing capacity fade vs polysulfide SOC range.—Chemical stability of the aqueous polysulfide electrolyte across the SOC range tested is a necessary condition for reversible electrochemical cycling. Before evaluating the stability of polysulfide electrolytes cycled to precipitation, we cycled the present electrolytes over various SOC ranges. The chemical equilibria in and stability of polysulfide species in aqueous solution were thoroughly studied in the 1970s and 1980s.[18,22,23,25–29] Licht et al.[22] and Giggenback[28] suggested that polysulfide species in aqueous media decay when cycled outside oxidation states bounded by S_4^{2-} and S_2^{2-}. Two fade mechanisms were proposed: one involves sulfide (S^{2-}) taking up protons to release H_2S while the other involves longer-chain polysulfide (S_5^{2-}) reacting with the hydroxide ion to form thiosulfate ($S_2O_3^{2-}$) as written in Eqs. 3 and 4, respectively. Both reactions result in capacity fade since H_2S gas is released, and thiosulfate formation is irreversible. Increasing the pH suppresses H_2S generation by reducing the available protons. The case of thiosulfate formation, however, is more complicated. As pH increases, the chemical equilibrium of polysulfide species favors short-chain polysulfides (i.e. S_4^{2-}, S_2^{2-}, or even S^{2-}); therefore, one of the reactants, OH^-, increases while the other, S_5^{2-}, decreases. The kinetics of thiosulfate formation, therefore, peaks at some intermediate pH. Calculations by Giggenback indicate that such intermediate pH occurs between pH of 12 and 14 depending on the overall oxidation state and the total sulfur concentration.[28] Furthermore, sulfur redox reaction in aqueous media has a standard electrode potential of −0.45 V vs the standard hydrogen electrode (SHE), which makes a high pH necessary to prevent hydrogen evolution during sulfur oxidation. To avoid these two fade mechanisms, all experiments in this study were conducted using 3 M NaOH as the supporting electrolyte, achieving pH > 14.

$$S^{2-}(aq) + 2\,H^{+}(aq) \rightarrow H_2S\,(g) \qquad [3]$$

$$S_5{}^{2-}(aq) + 3\;\; OH^{-}(aq) \rightarrow S_2O_3{}^{2-}(aq) + 3\,HS^{-}(aq) \qquad [4]$$

One way to increase the capacity density of the aqueous sulfur electrolyte is to access a wider range of sulfur capacity, illustrated as the vertical axis in Fig. 1b. To compare the r eversibility of aqueous polysulfide electrodes accessing different ranges of sulfur capacity, cycling experiments with 1 M Na_2S_4, equivalent to 4 M total sulfur, were conducted over capacities corresponding to the composition ranges Na_2S_2 to Na_2S_4, Na_2S_2 to Na_2S_6, and $Na_2S_{1.5}$ to Na_2S_4. These capacity ranges correspond to utilization of 25.0%, 33.3%, and 41.7% of the sulfur theoretical capacity, respectively (Fig. 1b). Cycling results are shown in Fig. 2. Since the known fade mechanisms are chemical rather than electrochemical in nature, we believe that the calendar time before observable decay is more indicative of stability than the number of cycles. The cell cycled between Na_2S_2 to Na_2S_4 (Fig. 2a) shows no detectable capacity fading throughout the 600 h duration of the experiment. The cells cycled over a wider range of capacity, Na_2S_2 to Na_2S_6 (Fig. 2b) and $Na_2S_{1.5}$ to Na_2S_4 (Fig. 2c), show increased polarization during oxidation by 450 h and 300 h of cycling, respectively. These results

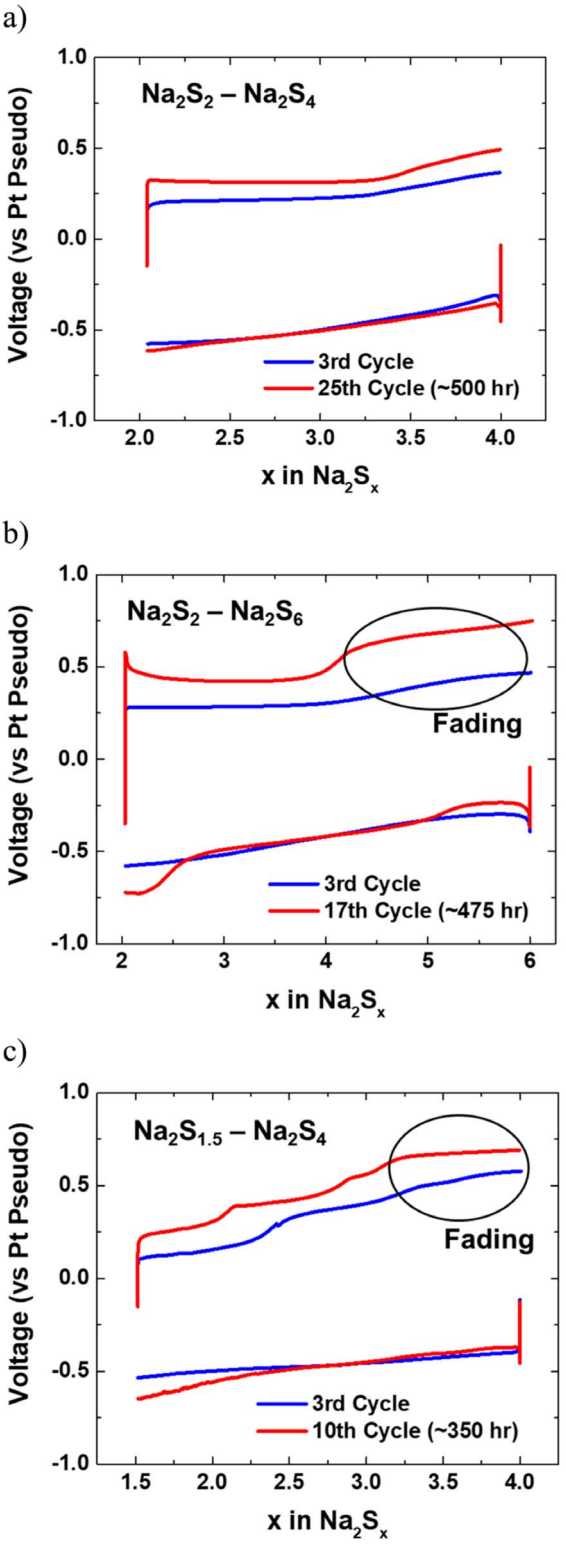

Figure 2. Electrochemical cycling of aqueous polysulfide electrolytes with 4 M sulfur concentration (1 M Na_2S_4) over various SOC swings: (a) Na_2S_2 to Na_2S_4, (b) Na_2S_2 to Na_2S_6, (c) $Na_2S_{1.5}$ to Na_2S_4. Chemical decay mechanisms discussed in the text cause degradation beyond 300 h of cycling time when sulfur is either oxidized or reduced outside the Na_2S_2–Na_2S_4, range, detected as an increase in polarization and/or appearance of an additional oxidative plateau. Experiments conducted at room temperature using 3 M NaOH supporting salt in modified H-cells using stainless steel electrodes and 0.2 mm thick Nafion 117 separator.

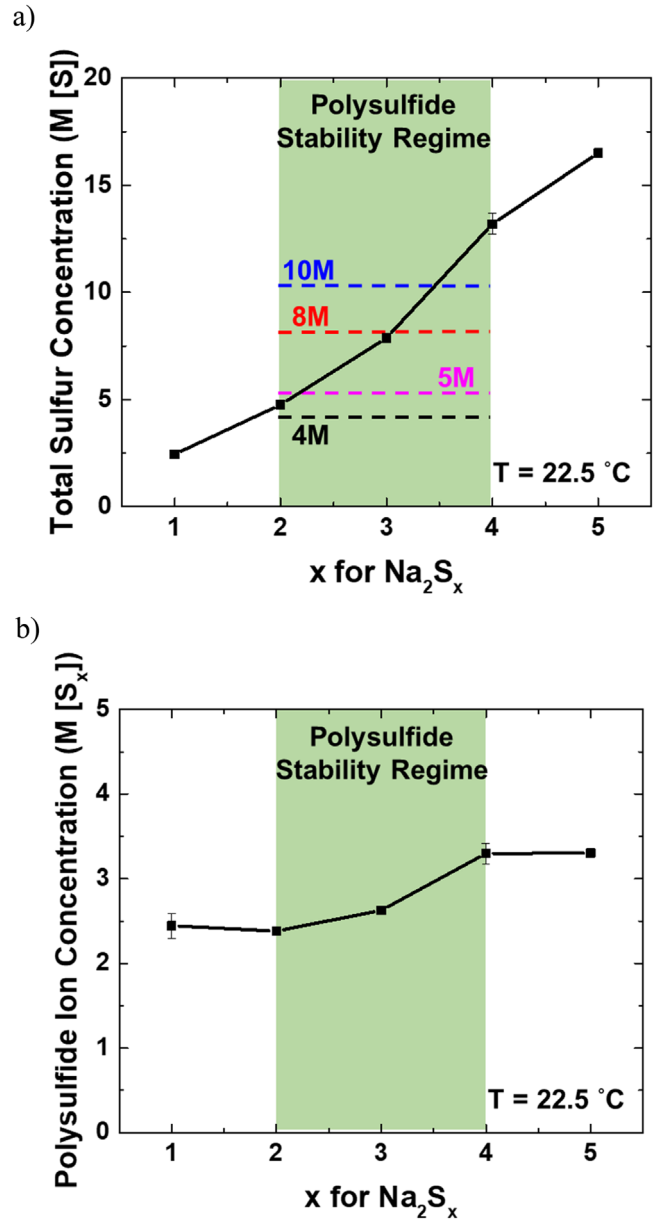

Figure 3. Variation in sodium polysulfide solubility as a function of overall state of reduction, corresponding to compositions Na_2S_x. The solid data points are the measured solubility at 22.5 °C in 3 M NaOH supporting electrolyte. The shaded band denotes the Na_2S_2—Na_2S_4 speciation regime over which cycling occurs without evident chemical degradation (see Fig. 2). (a) Solubility plotted in terms of total sulfur concentration. (b) Solubility plotted in terms of polysulfide ion concentration. As indicated in (a), 4 M, 8 M, and 10 M sulfur concentrations were examined in this study; 5 M is the limiting concentration for maintaining a completely soluble electrolyte within the Na_2S_2—Na_2S_4 cycling window.

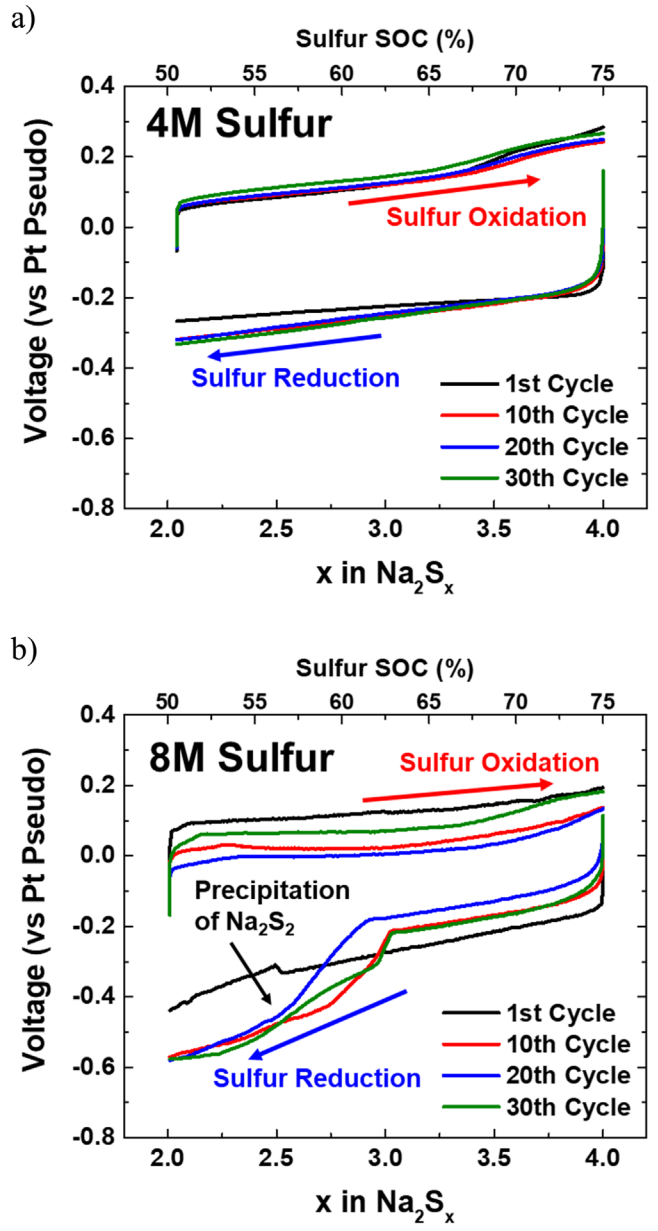

Figure 4. Cell voltage (vs a Pt pseudo reference electrode) vs composition for up to 30 cycles of aqueous polysulfide electrolytes with (a) 4 M sulfur (1 M Na_2S_4) and (b) 8 M sulfur (2 M Na_2S_4) concentration, both cycled within the speciation range Na_2S_2 to Na_2S_4. The 4 M sulfur electrolyte remains a single-phase liquid throughout. The 8 M sulfur electrolyte undergoes reversible sodium polysulfide precipitation and re-dissolution during cycling, as indicated by the voltage inflections, but nonetheless exhibit high reversibility beyond 30 cycles. Galvanostatic current density is 0.79 mA cm^{-2}, corresponding to C/11 rate at 4 M and C/21 rate at 8 M. Experiments conducted at room temperature using 3 M NaOH supporting salt in modified H-cells using stainless steel electrodes and 1 mm thick NaSICON separator. Results are corrected for the potential drop due to the resistance of the solid electrolyte.

showing instability when sulfur is cycled to both lower and higher oxidation states outside the Na_2S_2-Na_2S_4 window are consistent with the studies by Licht et al. and Giggenback, showing that S^{2-} and S_5^{2-} trigger H_2S generation and thiosulfate formation respectively.[22,28] Accordingly, subsequent cycling experiments in the present work were limited to the Na_2S_2-Na_2S_4 window.

Polysulfide solubility vs oxidation state.—The experiments showed that the solubility limit of sodium polysulfide increases with polysulfide oxidation state, Fig. 3. Here, the solubility is plotted in terms of both the total sulfur concentration (Fig. 3a) and polysulfide ion concentration (Fig. 3b), against stoichiometry x (in Na_2S_x), with the data points representing the experimental measurements and the green shaded area indicating the stable cycling range from Na_2S_2 to Na_2S_4. Within the range tested, the solubility measured in terms of total dissolved sulfur increases six-fold as the sulfur chains become longer, from around 2.5 M at Na_2S to >16 M at Na_2S_5 (to the right in Fig. 3a), but varies by less than a factor of two on a per-polysulfide ion basis (Fig. 3b). In the conventional design scheme for RFB electrolytes where complete solubility is desired, the maximum sulfur concentration would be

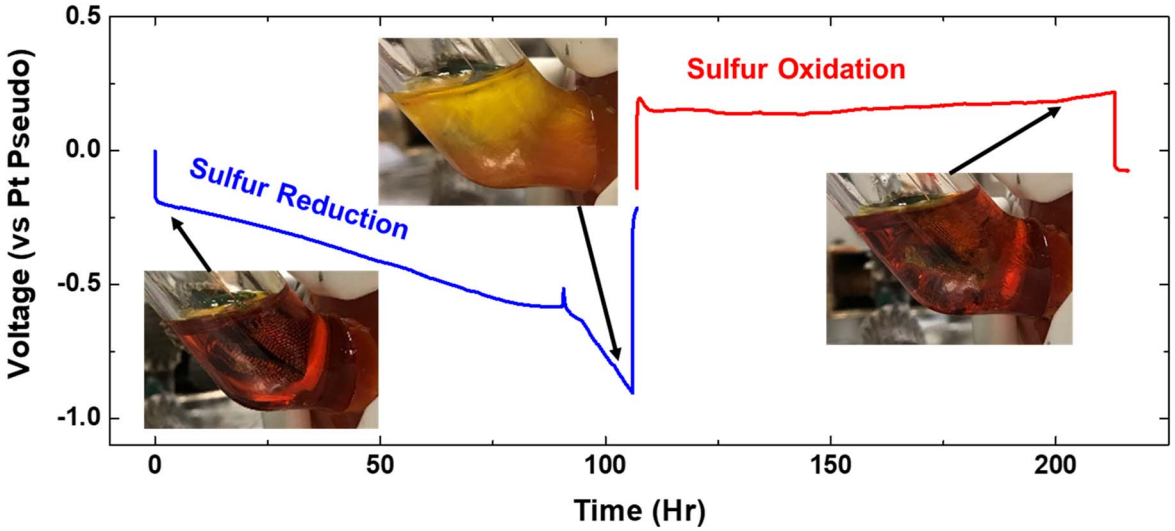

Figure 5. Reversible precipitation of sodium polysulfide during electrochemical cycling. The cell voltage (vs a Pt pseudo reference electrode) is shown against time for one galvanostatic cycle of a 2 M Na_2S_4 + 3 M NaOH electrolyte. Inset photographs show the appearance of the electrolyte at time points indicated. The sample is initially a uniform fully dissolved solution, but precipitates sodium sulfide as reduction proceeds. The precipitate is fully dissolved again upon oxidation. Experiment conducted at room temperature using 1.97 mA cm^{-2} current density (C/106 rate) in modified H-cell using stainless steel electrodes and a 1 mm thick NaSICON separator. Results are corrected for the potential drop due to the resistance of the solid electrolyte.

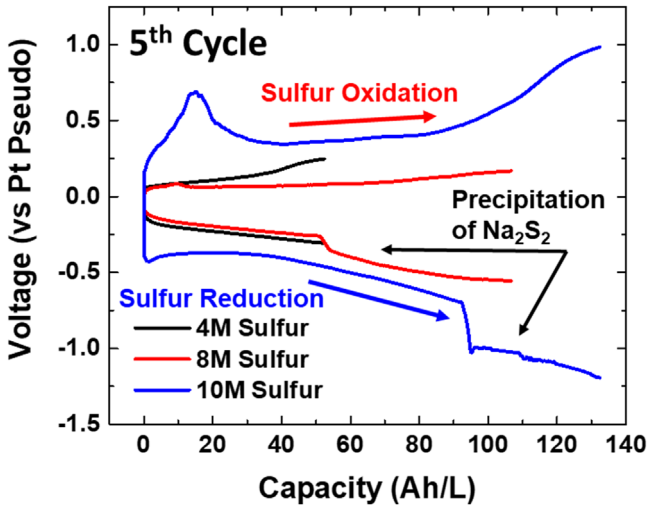

Figure 6. Cell voltage (vs a Pt pseudo reference electrode) vs capacity density (Ah/L) for 5th oxidation and reduction cycles of aqueous polysulfide electrolytes with 4 M, 8 M, and 10 M sulfur concentration. The 4 M S electrolyte is cycled entirely within its solution regime. The 8 M and 10 M S electrolytes exhibit voltage inflections upon reduction when Na_2S_2 precipitates, at ~50 Ah/L and ~90 Ah/L, respectively. Results obtained at room temperature and 0.79 mA/cm^2 current density using stainless steel electrodes and an 1 mm thick NaSICON separator. Results are corrected for the potential drop due to the resistance of the solid electrolyte.

5 M, corresponding to 67 Ah l^{-1} capacity density. However, if precipitation is allowed, and only in the fully oxidized limit of Na_2S_4 is complete solubility required, the maximum sulfur concentration becomes 13 M, corresponding to 175Ah l^{-1} capacity. Notably, there are other redox chemistries that exhibit similar variations in solubility between reduced and oxidized species. For example, for the polyiodide I^-/I_3^- redox couple, NaI has solubility as high as 7.8 M in aqueous solution while NaI_3 has a low solubility of <0.2 M.[10] The solubility limit of sodium polysulfide is expected to increase further with increasing temperature, allowing batteries using fully-dissolved polysulfides as well as the present scheme to access still higher sulfur concentrations.

Stability of polysulfides upon electrochemical cycling into the precipitation regime.—Based on the measured solubilities in Fig. 3a, we chose experimental sulfur concentrations of 4 M, 8 M, and 10 M for cycling experiments in which the starting Na_2S_4 solution is completely soluble. The 4 M composition should remain completely soluble upon reduction to Na_2S_2, while the 8 M and 10 M compositions should precipitate solid sodium polysulfide. Figure 4a shows voltage-composition cycling curves for the 4 M electrolyte, in which smooth curves without inflections indicative of precipitation are seen upon cycling to 30 cycles at C/11. For the 8 M electrolyte, Fig. 4b, a stepwise increase in polarization is observed upon reduction at ~Na_2S_3 composition, very close to the solubility limit for this composition shown in Fig. 3a. At the current rate for this experiment of C/21, it appears that precipitation upon electrochemical reduction occurs near the equilibrium solubility limit. An increase in polarization is commonly observed in electrochemically-induced precipitation since a nucleation barrier must be overcome, which requires a greater overpotential. However, during oxidation of the precipitated electrolyte, a smooth voltage curve is observed even though the precipitation reaction is being reversed. This is consistent with the general phase transformation principle that unlike exsolution, dissolution is barrierless. Stable galvanostatic cycling of the 8 M composition in Fig. 4b was observed to 40 cycles at C/21 rate, representing 1600h of calendar time, at which point the test was stopped. Thus, in a non-flow cell configuration, the experiments show that deep cycling at C/21 rate (current density of 0.79 mA cm^{-2}) is feasible. For a flow battery architecture, a higher current density at the power stack would naturally be required to reach comparable C-rates, which could be achieved by operating at higher temperature or by using higher surface area electrodes. In either configuration, however, the sulfur half-cell can employ cycling beyond the solubility limit.

Precipitation and dissolution during electrochemical cycling of the 8 M electrolyte was directly observed, Fig. 5. Here, the inset photos show the larger-volume H-cell in the as-assembled state, after reduction to Na_2S_2, and after oxidation back to Na_2S_4. At the beginning and end of this electrochemical cycle, the electrolyte has a transparent dark orange appearance. After reduction to Na_2S_2, a light yellow solid phase is clearly visible. This experiment was conducted at C/106 rate, while reversible cycling at C/21 rate is shown in Fig. 4b. These results confirm that equilibration between the precipitate and the solution is sufficiently fast to permit use of

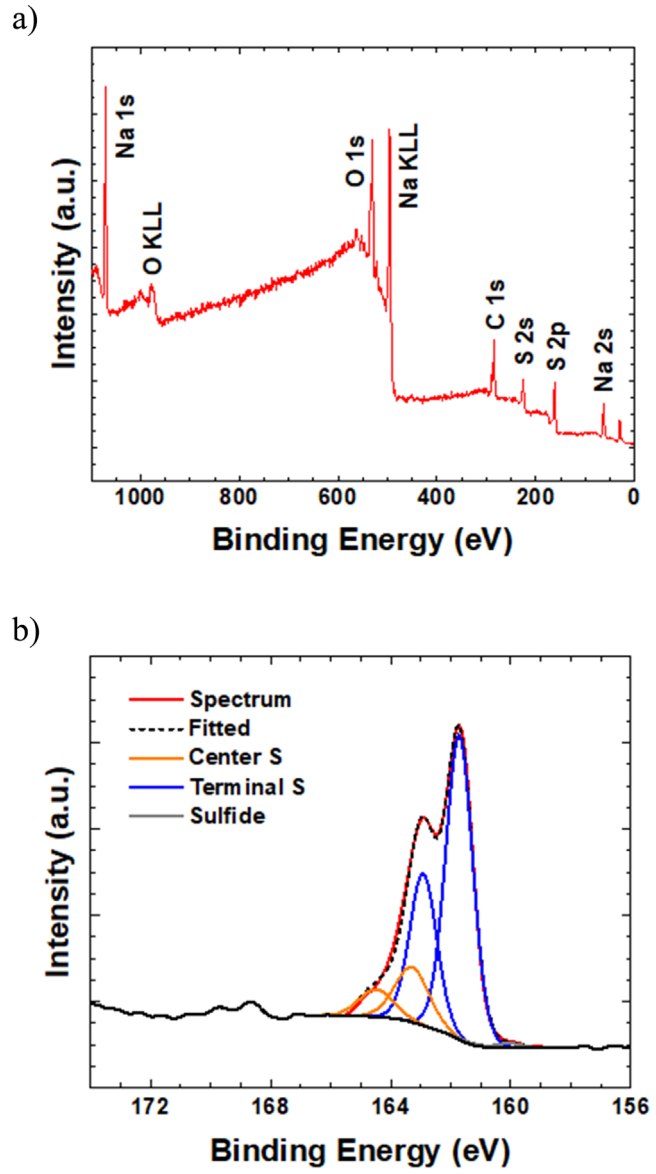

Figure 7. XPS spectra for sodium polysulfide precipitate extracted at the end of the reduction pulse in Fig. 5, corresponding to an electrode composition of Na_2S_2. a) survey spectrum, and b) S 2p spectrum. The S 2p spectrum allows chemical environment analysis for sulfur atoms, corresponding to the results tabulated in Table I. Scaling by the atomic percentages and the charge attributable to sodium ions in each chemical environment (i.e., Na-S-Na contributes +2 charge, Na-S-S contributes +1 charge, and S-S-S contributes none), the sulfur average oxidation state is calculated to be −0.82, corresponding to a nominal sulfide composition of $Na_2S_{2.4}$.

such electrolytes in batteries cycled over > 1 day duration. However, in preparing the polysulfide solutions, we found that even the 10 M electrolyte could be fully homogenized with stirring at room temperature from the starting Na_2S and sulfur powder within ~3 h. Equilibration of precipitated solutions on this time scale suggests that our proposed approach of reversible precipitation could be used in batteries for shorter storage durations, such as time-shifting renewable energy by a few hours.

At a higher electrolyte sulfur concentration of 10 M, the benefits of precipitation were diminished. Figure 6 compares 5th-cycle voltage-capacity density curves for the 4 M, 8 M and 10 M electrolytes. While the 8 M electrolyte shows about twice the capacity density of the 4 M electrolyte with similar polarization (107 Ah l^{-1} vs 67 Ah l^{-1}), and the 10 M electrolyte has proportionally higher capacity density (134 Ah l^{-1}), the latter also shows much greater polarization than either of the lower concentration electrolytes, even within the soluble regime. A larger polarization step is also observed upon precipitation. We believe that the higher resistance within the 10 M electrolyte may result from the consumption of liquid water in a solid hydrate upon precipitation, as discussed below.

Table I. XPS analysis of electrochemically precipitated sodium sulfide. Sulfur $2p_{3/2}$ peak positions, FWHMs, and corresponding atomic percentage of the sulfur environments Na-S-Na, Na-S-S, and S-S-S are shown.

Feature	Na-S-Na	Na-S-S	S-S-S
S $2p_{3/2}$ Position (eV)	160.0	161.7	163.3
S $2p_{3/2}$ FWHM (eV)	1.00	1.06	1.35
Atomic percentage	0.93	80.49	18.48

Characterization of sodium polysulfide precipitate.—Precipitates extracted from the cell shown in Fig. 5 after reduction, and dried as described in the Experimental section, were examined by SEM. A smooth micron-scale morphology was observed, Fig. S2, with no significant distinguishing features. X-ray diffraction showed a complex multiphase assemblage in which individual phases were difficult to identify. We turned to XPS for further characterization of the precipitate. XPS has been widely used to study sulfur-based compounds, in part due to the availability of binding energy information for sulfur in different chemical environments (separation of about 8 eV from sulfate S^{6+} to sulfide S^{2-}). Fantauzzi et al.[24] explored XPS studies of minerals and alkali metal polysulfide using the S 2p peaks and S KLL peaks, and Swamy et al. have investigated the decomposition reactions of LiP_2S_5 driven to extreme potentials using XPS.[30] XPS has also been used to investigate sulfur chemistry evolution in Li-S batteries and sulfide-based solid-state electrolytes in Li-ion batteries.[31,32] Here, we obtained XPS spectra from polysulfide precipitate extracted immediately after electrochemical reduction, Fig. 7. The survey spectrum (Fig. 7a) include all elements expected, sodium, sulfur, and oxygen, as well as carbon, attributed to surface contamination. The relatively strong oxygen peak, combined with only weak sulfate and sulfite peaks (binding energy ~169 eV) in the S 2p spectra to which the oxygen could be attributed, Fig. 7b, suggest that the precipitate is a hydrate rather than a pure sulfide. The sulfide component can be further interpreted. The S 2p spectrum showed overlap of multiple S $2p_{3/2}$-S $2p_{1/2}$ doublets. Each doublet consists of two peaks constrained to binding energy separation of 1.2 eV and intensity ratio of S $2p_{3/2}$:S $2p_{1/2}$ = 2:1. Alkali metal sulfide chains have their sulfur atoms in three possible chemical environments: Na-S-Na, Na-S-S, and S-S-S. Here, Na-S-Na represents the Na_2S phase, while Na-S-S corresponds to terminal sulfur and S-S-S corresponds to center sulfur along a polysulfide chain. Table I summarizes the binding energy and full width at half maximum (FWHM) for the S $2p_{3/2}$ peak as well as the atomic percent for sulfur in the three chemical environments. The three doublets with S $2p_{3/2}$ binding energy at 160.0 eV, 161.7 eV, and 163.3 eV, are assigned to Na-S-Na, Na-S-S, and S-S-S, respectively. Both peak positions and FWHM values agree well with those reported in Fantauzzi et al.[24] The atomic percentage of sulfur in each of the three chemical environments can be calculated using the ratio of areas under the doublets. We find that the precipitate consists of 0.9% sulfide, 80.5% terminal sulfur, and 18.5% center sulfur. From this result, the average composition of the polysulfide can be deduced. Assuming that in accordance with previous literature[12] Na_2S_3 is not present and only Na_2S_2 (Na-S-S-Na) and Na_2S_4 (Na-S-S-S-S-Na) are possible, it can be concluded that at least 62% of the sulfur in the freshly reduced precipitate is in the form of Na_2S_2. That is, since center sulfur predominantly belongs to Na_2S_4, the

percentage of sulfur present as Na_2S_4 is $2 \times 18.5\% = 37.0\%$ of sulfur leaving 62.0% of sulfur to Na_2S_2. Any longer-chain polysulfides present would push the Na_2S_2 percentage to still higher value. Therefore, we conclude that the precipitate is predominantly Na_2S_2.

The atomic percentages from XPS also allow for independent calculation of the average oxidation state of sulfur in the precipitate. We do this by counting the charge attributed to sodium ions, wherein Na-S-Na contributes +2 charge, Na-S-S contributes +1 charge, and S-S-S contributes none. Scaling by the percentage of each environment, we obtain a sulfur average oxidation state of −0.82, which corresponds to a nominal sulfide composition of $Na_2S_{2.4}$.

Conclusions

We show that aqueous sodium polysulfide electrolytes have strongly state-of-charge dependent polysulfide solubility, yet can be electrochemically cycled between the fully-soluble and precipitated regimes without losing reversibility. Taking advantage of the precipitated charge storage regime allows increased energy density and lower storage cost compared to completely soluble electrolytes, and may be especially useful for long-duration storage applications where C-rates are slow enough to allow equilibration between precipitated solid and saturated redox-active solution. An 8 M sulfur alkaline electrolyte precipitates below ∼50% state-of-charge at room temperature, yet exhibits >30 full SOC cycles over >1600h of calendar time with negligible capacity fade, doubling the capacity density of a 4 M completely soluble counterpart. XPS analysis of the electrochemically precipitated solid shows that it is predominantly a hydrated Na_2S_2. Technoeconomic analysis indicates that this change alone reduces the chemical cost of capacity storage by 30% for a polysulfide electrode. This approach may be generalizable to other solution-based electrolytes, and may be used in both static cell and flow cell architectures.

Acknowledgments

This work was supported as part of the Joint Center for Energy Storage Research, an Energy Innovation Hub funded by the U.S. Department of Energy, Office of Science, Basic Energy Sciences. This work made use of the MRSEC Shared Experimental Facilities at MIT, supported by the National Science Foundation under award number DMR-1419807.

ORCID

Andres F. Badel https://orcid.org/0000-0002-0958-8969
Fikile R. Brushett https://orcid.org/0000-0002-7361-6637
Yet-Ming Chiang https://orcid.org/0000-0002-0833-7674

References

1. Revolution Now, U.S. Department of Energy, The future arrives for five clean energy technologies Update, U.S. Department of Energy (2015), https://www.energy.gov/eere/downloads/revolution-now-future-arrives-five-clean-energy-technologies-2015-update.
2. S. Chu, Y. Cui, and N. Liu, *Nature Mater*, **16**, 16 (2017).
3. B. Dunn, H. Kamath, and J.-M. Tarascon, *Science*, **334**, 928 (2011).
4. Z. Yang, J. Zhang, M. C. W. Kintner-Meyer, X. Lu, D. Choi, J. P. Lemmon, and J. Liu, *Chem. Rev.*, **111**, 3577 (2011).
5. G. L. Soloveichik, *Chem. Rev.*, **115**, 11533 (2015).
6. W. A. Braff, J. M. Mueller, and J. E. Trancik, *Nat. Clim. Change*, **6**, 964 (2016).
7. J. A. Ober, "Mineral commodity summaries 2017." *U.S. Geological Survey Reston*, (2017).
8. S. H. Ge, B. L. Yi, and H. M. Zhang, *J. Appl. Electrochem.*, **34**, 181 (2004).
9. R. Zito, "Process for energy storage and/or power delivery with means for restoring electrolyte balance." *US Patent No.* 5612148 (1997).
10. L. Su, A. F. Badel, C. Cao, J. J. Hinricher, and F. R. Brushett, *Ind. Eng. Chem. Res.*, **56**, 9783 (2017).
11. Z. Li, G. Weng, Q. Zou, G. Cong, and Y.-C. Lu, *Nano Energy*, **30**, 283 (2016).
12. X. Wei, G.-G. Xia, B. Kirby, E. Thomsen, B. Li, Z. Nie, G. G. Graff, J. Liu, V. Sprenkle, and W. Wang, *J. Electrochem. Soc.*, **163**, A5150 (2016).
13. N. Li, Z. Weng, Y. Wang, F. Li, H.-M. Cheng, and H. Zhou, *Energy Environ. Sci.*, **7**, 3307 (2014).
14. R. Demir-Cakan, M. Morcrette, J.-B. Leriche, and J.-M. Tarascon, *J. Mater. Chem. A*, **2**, 9025 (2014).
15. R. Demir-Cakan, M. Morcrette, and J.-M. Tarascon, *J. Mater. Chem. A*, **3**, 2869 (2015).
16. Z. Li, M. S. Pan, L. Su, P.-C. Tsai, A. F. Badel, J. M. Valle, S. L. Eiler, K. Xiang, F. R. Brushett, and Y.-M. Chiang, *Joule*, **1**, 306 (2017).
17. D. Peramunage and S. Licht, *Science*, **261**, 1029 (1993).
18. S. Licht, *J. Electrochem. Soc.*, **134**, 2137 (1987).
19. S. J. Visco, Y. S. Nimon, B. D. Katz, L. C. De Jonghe, N. Goncharenko, and V. Loginova, "Aqueous electrolyte lithium sulfur batteries." U.S. Patent No. 8828575B2 (2014).
20. U.S. Department of Energy, *Long Duration Storage Shot* (2021), https://www.energy.gov/eere/long-duration-storage-shot.
21. D. J. O'Brien and F. B. Birkner, *Environ. Sci. Technol.*, **11**, 1114 (1977).
22. S. Licht, G. Hodes, and J. Manassen, *Inorg. Chem.*, **25**, 2486 (1986).
23. W. Giggenbach, *Inorg. Chem.*, **11**, 1201 (1972).
24. M. Fantauzzi, B. Elsener, D. Atzei, A. Rigoldi, and A. Rossi, *RSC Adv.*, **5**, 75953 (2015).
25. W. Giggenbach, *Inorg. Chem.*, **10**, 1333 (1971).
26. S. Licht, *J. Electrochem. Soc.*, **135**, 2971 (1988).
27. W. F. Giggenbach, *Inorg. Chem.*, **13**, 1724 (1974).
28. W. F. Giggenbach, *Inorg. Chem.*, **13**, 1730 (1974).
29. S. Licht, J. Manassen, and G. Hodes, *J. Electrochem. Soc.*, **133**, 272 (1986).
30. T. Swamy, X. Chen, and Y.-M. Chiang, *Chem. Mater.*, **31**, 707 (2019).
31. Y. Fu, Y.-S. Su, and A. Manthiram, *Angew. Chem. Int. Ed.*, **52**, 6930 (2013).
32. S. Wenzel, S. Randau, T. Leichtweiß, D. A. Weber, J. Sann, W. G. Zeier, and J. Janek, *Chem. Mater.*, **28**, 2400 (2016).